2010

Study Of The Interactions Of Proteins, Cells And Tissue With Biomaterials

Abhijeet Bhalkikar
University of Central Florida

STUDY OF THE INTERACTIONS OF PROTEINS, CELLS AND TISSUE WITH BIOMATERIALS

by

ABHIJEET BHALKIKAR
B.S. University of Pune, India, 2002

A thesis submitted in partial fulfillment of the requirements
for the degree of Master of Science
in the Department of Electrical Engineering and Computer Science
in the College of Engineering and Computer Science
at the University of Central Florida
Orlando, Florida

Summer Term
2010

ABSTRACT

Bioengineering is the application of engineering principles to address challenges in the fields of biology and medicine. Biomaterials play a major role in bioengineering. This work employs a three level approach to study the various interactions of biomaterials with proteins, cells and tissue *in vitro*. In the first study, we qualitatively and quantitatively analyzed the process of protein adsorption of two enzymes to two different surface chemistries, which are commonly used in the field. In the second study, we attempted to engineer a tissue construct to build a biocompatible interface between a titanium substrate and human skin. In the third study, an *in-vitro* model of the motoneuron-muscle part of the stretch reflex arc circuit was developed. Using a novel silicon based micro-cantilever device, muscle contraction dynamics were measured and we have shown the presence of a functional neuro-muscular junction (NMJ). These studies have potential applications in the rational design of biomaterials used for biosensors and other implantable devices, in the development of a functional prosthesis and as a high-throughput drug-screening platform to study various neuro-muscular disorders.

TABLE OF CONTENTS

LIST OF FIGURES

LIST OF TABLES

INTRODUCTION

Biomaterials are an integral part of bioengineering. By their definition they are "any material that is either natural or man-made which comprises whole or part of a living structure or a biomedical device that performs, augments or replaces a natural function in our body". When implanted in the body, biomaterials come in contact with blood, proteins, cells and tissues. Each of these components has very specific interactions with the biomaterial. The goal of this thesis was to study and quantify some of these interactions using different parameters and materials.

Chapter 1 is dedicated to the study of protein interactions with certain biomaterials. A surface interaction is the interaction between a protein and biomaterial and is controlled by a variety of factors. Factors include the surface chemical moieties of the biomaterial involved, the structure and sequence of the protein, as well as the pH and ionic strength of the buffer solution used. In this study, the adsorption of two enzymes glucose oxidase and horseradish peroxidase, were quantified on two different surface composition, a fluorinated surface that is hydrophobic in nature and a glass surface that is hydrophilic. The quantification was achieved by using both X-ray photoelectron spectroscopy (XPS) and micro-BCA assay, which are complementary methods. The absolute quasi-equilibrium surface coverage using both techniques was calculated. The affinity constants (Ka) for the proteins to the surface were also calculated using a simple Langmuir adsorption model equation. Both techniques produced comparable results. Also, the qualitative difference in the adsorption on the two compositions is also discussed.

In chapter 2, the interaction between a tissue and biomaterial was studied by creating a tissue engineered construct to build a bridge between titanium and human skin. This has potential application in the development of a fully osseo-integrated artificial limb. A novel polycaprolactone based tissue-engineering construct, was developed and then printed on a titanium substrate using a computer assisted bio-printing tool. This construct was then optically and mechanically characterized to determine the adhesive strength of the construct to the substrate. Human dermal fibroblast cells were then plated on the construct and their viability was assessed after several days in culture. In order to prevent bacterial infection at the interface, the construct was also seeded with 3 different anti-bacterial agents viz., silver nanoparticles, titanium dioxide anatase and chlorhexidine diacetate. The efficacy of these agents was then assessed by observing the viability of *Staphylococcus aureus* bacteria, which were plated on these constructs. Results indicated that the construct provided excellent mechanical properties similar to skin, was viable for fibroblast cells and exhibited very good antibacterial properties with the chlorhexidine diacetate.

In chapter 3, the interaction between cells and biomaterials was investigated. The development of an *in-vitro* model of the stretch reflex arc circuit in our body was attempted. In this embryonic rat skeletal and spinal cord motoneuron cells were co-cultured on a special bio-MEMS, silicon based, cantilever device under defined conditions. The cantilever device was then fixed in a unique AFM detection system. An electric field stimulation of a defined voltage and frequency was applied to the co-culture and the synchronous contraction of the muscle cells was observed. This allows the study of the muscle force dynamics. The formation of a functional neuro-muscular junction

(NMJ) was shown by interrogating the system with glutamate, which is an excitatory neurotransmitter. This induced the muscle to undergo contraction by the motoneuron but the blocking of the NMJ using a cholinergic agonist was not observed. The application of the glutamate to a pure muscle culture elicited no response. This system has potential in a high throughput drug-screening platform for neuro-muscular diseases.

CHAPTER 1
ADSORPTION BEHAVIOR OF TWO PROTEINS ON FLUORINATED AND GLASS SURFACES STUDIED USING A COMBINATION OF XPS AND PROTEIN COLORIMETRIC ASSAY

Introduction

The structural changes of proteins at a solid-liquid interface are of great interest in bioengineering[1]. However, the measurements of the extent and the rate of protein conformational changes are very difficult.

In recent years, the interest in proteins has grown due to the development of new techniques in protein chemistry and major advances with more established techniques. The need for atomic level description of the structure and dynamics of proteins at interfaces has led to the development of new approaches in protein studies. X-ray Photoelectron Spectroscopy (XPS) is an excellent surface specific technique, which can be used to study the adsorbed proteins layers on different surfaces due to its high surface sensitivity and chemical selectivity[2]. Recently, more researchers are turning toward XPS to study cell culture and proteins on surfaces[3]. Extensive literature is available on the principles of XPS analytical procedures and instrumentation[4]. In addition, there are a few papers reporting on the qualitative and quantitative investigations of protein adsorption on different surfaces using XPS, ToF-SIMS and other techniques[5,6,7].

Researchers have studied immobilization and adsorption of glucose oxidase (GO) and horse-radish peroxidase (HRP) to surfaces using tools from analytical chemistry[8,9]. In this chapter, an additional analytical biochemical tool was provided to gain a better look at the behavior of proteins at interfaces and their structural changes upon adsorption. The biochemical assay used was the bicinchoninic acid colorimetric assay, which is very

sensitive in detecting very small amounts of protein and is commonly used for quantifying the total amount of protein[10]. The main aim of this work was to study the protein adsorption on a fluorinated hydrophobic surface (13F) and a hydrophilic clean glass surface to determine which physical properties of the protein or material are important in describing the mechanism of protein adsorption. The proteins used in the study were GO and HRP, both of which are widely used in biosensors[11,12]. In a previous study, the adsorption was carried out under static conditions[13]. The Langmuir adsorption isotherms were determined and data binding constants were calculated using a modified Langmuir adsorption isotherm equation for XPS and biochemical assay techniques. Both techniques produced comparable results.

Materials and Methods

Micro cover glasses (22x22 mm, VWR) were cleaned according to the published procedure[14] and used as substrates in all protein adsorption experiments. The hydrophobic surfaces were prepared by modifying clean glass with trichloro (1H,1H,2H,2H-perfluorooctyl) silane (13F) (Gelest Inc.). To assure the desired surface properties, contact angle and XPS were conducted and only samples with a contact angle below 5^{o} were used as hydrophilic surfaces and those with contact angles above 105° were used as hydrophobic surfaces.

Glucose oxidase (GO) (50 KU, Sigma-Aldrich) and immunopure horse-radish peroxidase (HRP) (100 mg, Pierce) were used in all protein adsorption experiments. The protein adsorption and desorption experiments were performed in 8 ml staining jars with 4 cover slips per jar for 2 hours at room temperature with mild agitation. The surfaces were immersed in phosphate buffer saline (PBS) buffer solution (Fisher-Scientific) (pH =

7.4) with protein concentrations ranging from 5 to 500 μg/ml. After adsorption, surfaces were removed, rinsed three times with PBS and once in water, and then air dried overnight. Washed and dried samples were examined using a Physical Electronics 5400 ESCA spectrometer.

The instrument was operated using a monochromatic Mg Ka X-ray source with a pass energy at 40 eV. The take-off angle was 90^{o}, and normal operating pressure was approximately 10^{-9} Torr. Survey and high-resolution energy spectra for silicon, oxygen, carbon, nitrogen, and fluorine were measured for each sample. The intensities of nitrogen N (1s) peaks at 400 eV and carbonyl peaks C (1s) at 287 eV, specific to protein peptide bonds, were calculated using an internal standard (after deconvolution and curve fitting peaks were normalized against the sum of the area under the curves of all the peaks) and the data were averaged for each sample using three different spots.

The representative XPS data was obtained for adsorption of a protein on 13F based on the nitrogen and carbonyl peaks, respectively. There was a correlation in the intensity changes between the data obtained using N or the carbonyl peak. It was very useful information for samples on which the presence of nitrogen on a surface cannot be associated exclusively with the presence of protein on the surface.

After protein adsorption, coverslips were exposed to the same amount of protein, transferred to glass jars (4 surfaces/glass jar) and incubated in 8 ml of 1% sodium dodecyl sulphate (SDS) (Sigma-Aldrich) solution overnight on a shaker at room temperature. After desorption, the surfaces were removed, dried and studied by XPS. The XPS data showed negligible nitrogen peaks indicating insignificant amounts of protein on the surfaces.

Next, the aliquots of solutions with an unknown amount of desorbed protein were transferred to a 96 well plate and quantified using the microBCA assay. The microBCA ™ protein assay kit was purchased from Pierce Ltd. and the working reagent was prepared according to the kit instructions. The protein standard was prepared by diluting the BSA stock solution (2.0 mg/ml) into the PBS (pH=7.4) buffer to achieve the desired concentration. Three sets of eight dilutions were made ranging in concentration from 0 - 40 μg/ml to prepare a standard curve. An example of a standard curve is shown in Figure 1.

150 ml each of the blank and unknown samples were all aliquoted onto the same micro plate in triplicate and 150 ml of the working reagent was then added to each well and mixed. The plate was then incubated (37^{o}C) for 2 hours. After incubation, the plate was cooled to room temperature and read at 562 nm using a BioTek Synergy HT multi detection microplate reader utilizing the KC4 software.

The optical density (OD) of the blanks was subtracted from the OD of the samples to obtain the net OD. The concentration of desorbed protein was estimated using a BCA standard curve and the % monolayer coverage on the surface was then calculated.

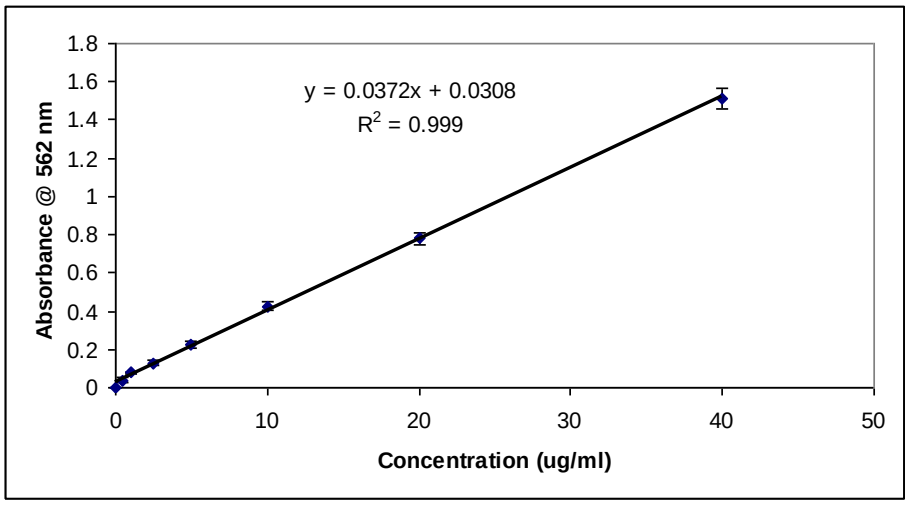

Figure 1. BCA standard curve using the BSA standards

Results and Discussion

Figures 2 and 3 represent the averaged Langmuir adsorption isotherm data based on the XPS analysis using the integrated area of nitrogen peaks for GO and HRP on 13F and glass, respectively.

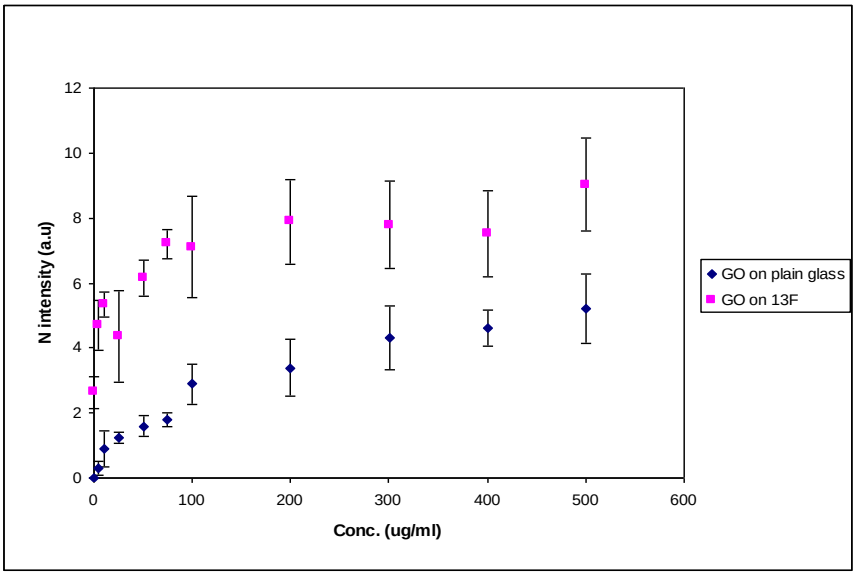

Figure 2. XPS data for GO adsorption on 13F and plain glass

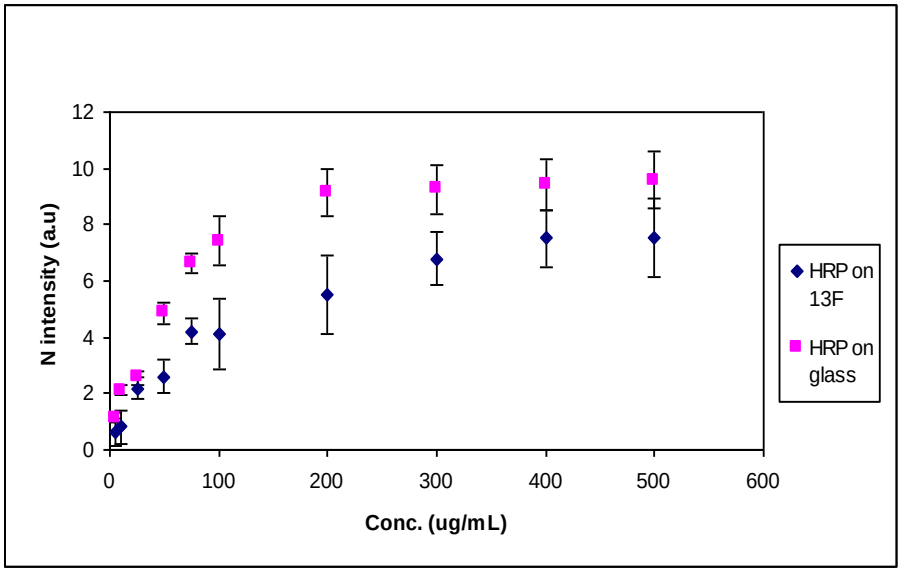

Figure 3. XPS data for HRP adsorption on 13F and plain glass

As previously described [13], to model the protein adsorption, a modified Langmuir adsorption isotherm was used, given by equation 1.

$$Q = KC / (1+KC) \quad (1)$$

where Q = monolayer coverage, K = adduct formation constant at steady-state, and C = molar concentration. The final state of adsorption is a reactive site limited adsorbed layer. Since $Q = N/N_m$, where N is the amount of material on the surface at a given concentration, and N_m is the amount on the surface at monolayer coverage, equation 1 can be rearranged to:

$$C/N = C/N_m + 1/KN_m \quad (2)$$

This is similar to the equation y = mx + c for a straight line, where m is the slope of the line and c is its y-intercept. Comparing the two equations, one gets y = C/N, x = C, m = 1/Nm and c = 1/KNm. Therefore, the binding constant K can be calculated by plotting C/N versus C and then determining the slope and y-intercept of the graph. The constant is then K = m/c. The amount of protein adsorbed on the surface can be determined from XPS analysis using the nitrogen peak or from the microBCA assay.

From Figures 2 and 3, it is clear that the data can be divided into two concentration regimes, with two linear regions with different slopes that can fit the data. The slope of each line is decreased with increasing analytical concentration of the protein

in solution. Therefore, the data was fitted to the adsorption isotherms separately for lower and higher protein concentrations in solution using Equation 2.

A representative fit for HRP adsorption on 13F is shown in Figures 4 and 5. The data indicates that at first HRP was adsorbed quickly to the surface with an average binding constant of $K_1 = 0.0166$. At a certain coverage, however, further adsorption of HRP was decreased due to the unavailability of binding sites. The second binding energy was therefore lower and equals $K_2 = 0.0068$. The data for GO adsorption has also shown a similar trend with K1 = 0.034 and K2 = 0.012, respectively.

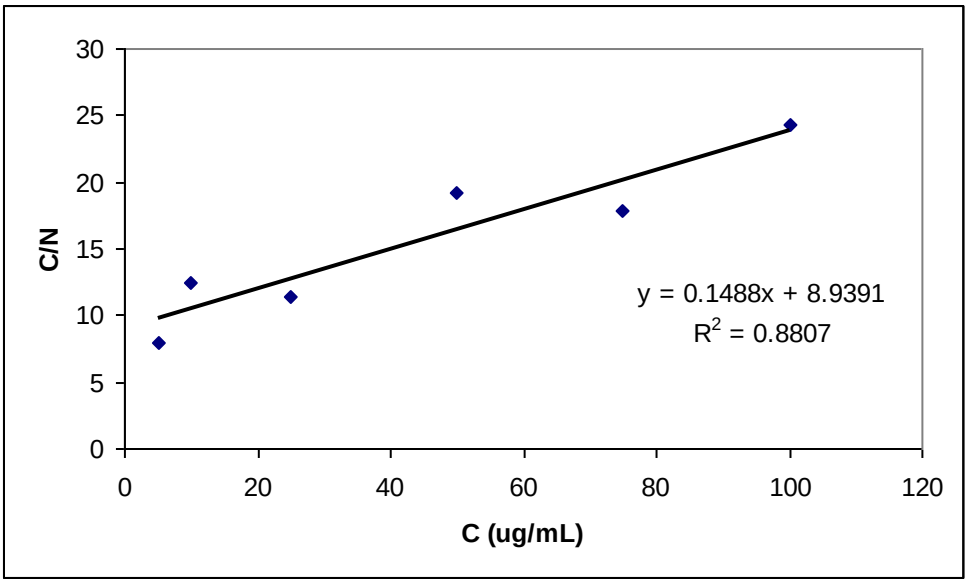

Figure 4. Calculation of a binding constant for HRP adsorption on 13F for lower concentrations

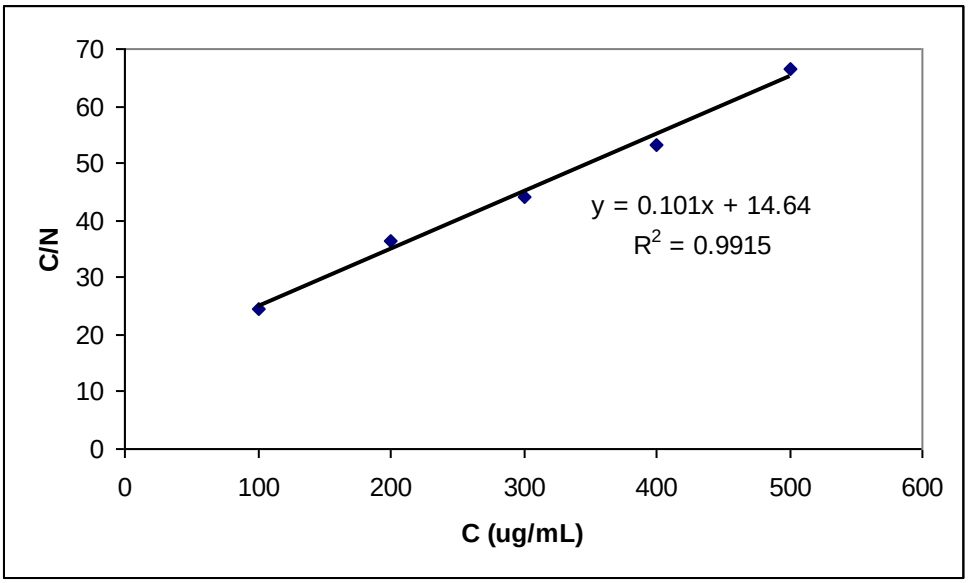

Figure 5. Calculation of a binding constant for HRP adsorption on 13F for higher concentrations

The example of a binding isotherm obtained for GO and HRP on clean glass using the microBCA assay is shown in Figures 6 and 7. The % monolayer coverage of the

proteins was calculated by assuming the molecular footprint area of GO and HRP to be ~56 nm^2 and ~40 nm^2, respectively[15,16]. The binding constants were calculated in a similar manner as indicated above. At lower concentrations both proteins adsorbed vigorously to the surface. At higher concentrations, adsorption proceeded at a slower rate.

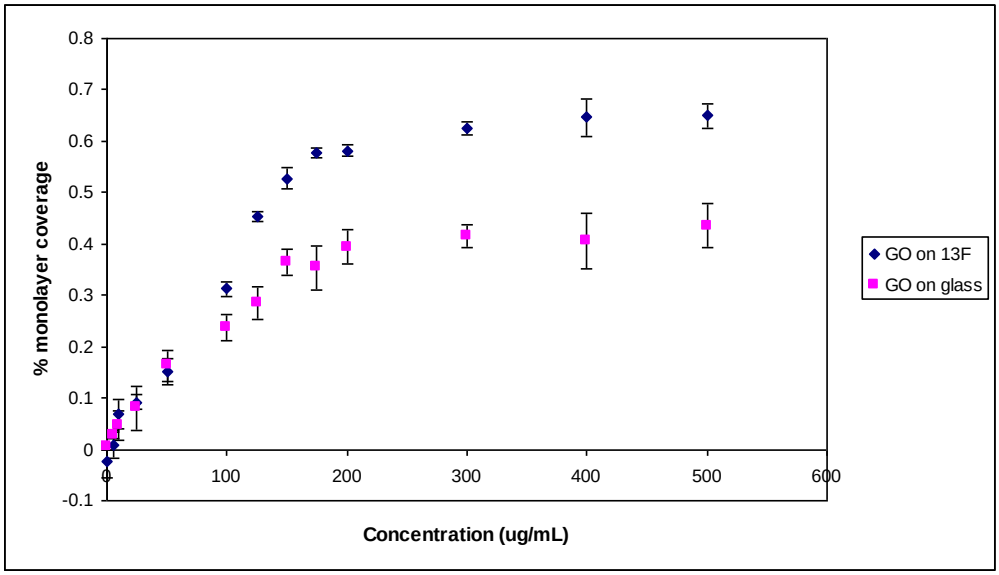

Figure 6. MicroBCA data for GO adsorption on 13F and plain glass

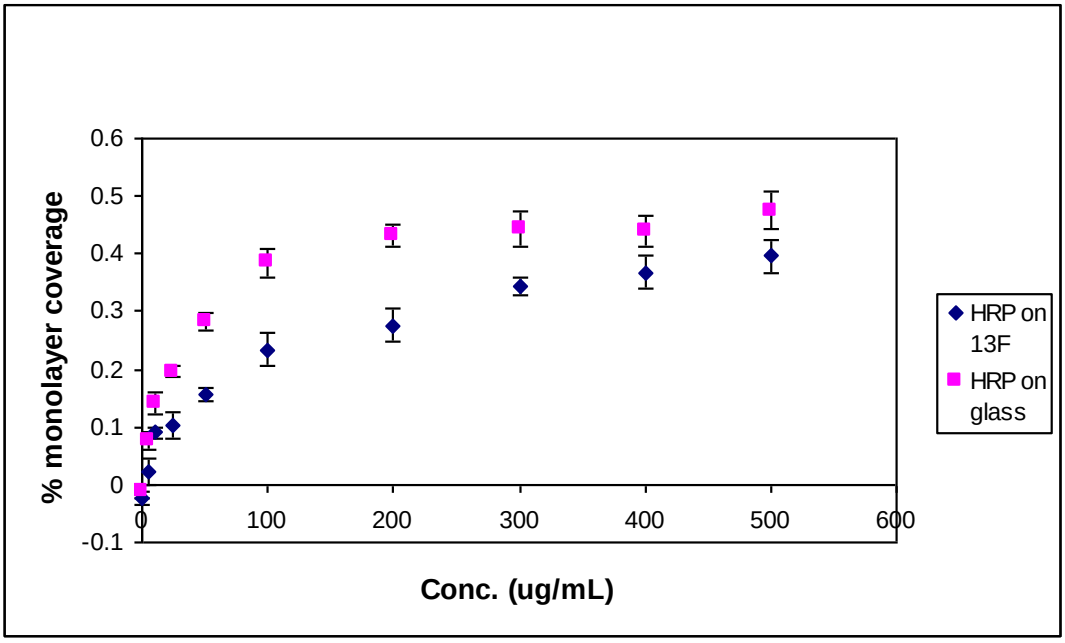

Figure 7. MicroBCA data for HRP adsorption on 13F and plain glass

The binding constants for both proteins on both surfaces are summarized in Table 1. It can be observed from the table that both XPS and microBCA data show the same adsorption behavior at higher concentrations, but for lower concentrations the binding constants that were calculated based on the microBCA method are lower compared to the XPS measurements. It is important, however, to point out that for lower concentrations the microBCA method is at its determination limits, and therefore, such a large discrepancy was observed for lower protein coverage.

Table 1. Values of binding constants for GO and HRP on 13F and glass

	XPS		MicroBCA assay	
	K1	K2	K1	K2
GO on 13F	0.034	0.012	0.019	0.009
GO on glass	0.023	0.018	0.015	0.012
HRP on 13F	0.017	0.006	0.012	0.003
HRP on glass	0.032	0.017	0.023	0.014

Another trend that can be observed from the data is that GO adsorption on 13F was greater than that on glass, while for HRP the adsorption was greater on glass than 13F. This can be attributed to the fact that the iso-electric point (pI) of GO is 4.2 and that of HRP is 7.2, so that in the buffer used GO is highly negatively charged and HRP is slightly charged. These different electrostatic interactions might explain the different adsorption profiles in regards to glass and 13F. Also, GO is a much larger protein (mol. weight 160 kDa) whereas HRP is smaller (40 kDa), which might lead to the different orientations of the protein on the surface, thus leading to different coverages. Both the XPS and microBCA data have shown the same trends.

Conclusion

The adsorption behavior of two test proteins on two different surfaces was observed. XPS is a very sensitive technique and can be used to detect very small amounts of an adsorbed protein. Another biochemical tool, the microBCA assay, was also used to look at the adsorption phenomena. Both techniques are complementary to each other and produced comparable results. The advantage of using the biochemical assay was its ease of use and expensive instrumentation such as an XPS setup, to look at protein adsorption to different surfaces is not necessary. This technique is useful to biologists, biochemists, surface chemists, and engineers.

References

1. K. Nakanishi, T. Sakiyama, K. Imamura, “On the adsorption of proteins on solid surfaces, a common but very complicated phenomenon”, Journal of Bioscience and Bioengineering, 2001, 91, 3, 233-244.
2. H. Fitzpatrick, P. F. Luckham, S. Eriksen and K. Hammond, “Use of x-ray photoelectron spectroscopy to study protein adsorption to mica surfaces”, Journal of Colloid and Interface Science, 1992, 149, 1, 1-9.
3. D. Jung, D. Cuttino, J. Pancrazio, P. Manos, T. Cluster, R. Sathanoori, L. Aloi, M. Coulombe, M. Czarnaski, D. Borkholder, G. Kovacs, P. Bey, D. Stenger, J.J. Hickman, “Cell-based sensor microelectrode array characterized by imaging x-ray photoelectron spectroscopy, scanning electron microscopy, impedance measurements, and extracellular recordings”, Journal of Vacuum Science & Technology A: Vacuum, Surfaces, and Films, 1998, 16, 3, 1183-1188.
4. M. Briggs, M. Seah, “Practical Surface analysis by Auger and X-ray Photoelectron Spectroscopy”, 1992, 2nd Ed., John Wiley& Sons, New York.
5. M. Henry, C. Dupont-Gillain, P. Bertrand, “Characterization of Insulin Adsorption in the presence of Albumin by Time-of-Flight Secondary Ion Mass Spectrometry and X-ray Photoelectron Spectroscopy”, Langmuir, 2008, 24, 458-464.
6. M. Wagner, S. McArthur, M. Shen, T. Horbett, D. Castner, “Limits of detection for time of flight secondary ion mass spectrometry (ToF-SIMS) and X-ray photoelectron spectroscopy (XPS): detection of low amounts of adsorbed protein”, Journal of Biomaterial Science Polymer Edition, 2002, 13, 4, 407-428.
7. M. Browne, G. Lubarsky, M. Davidson, R. Bradley, “Protein adsorption onto polystyrene surfaces studied by XPS and AFM”, Surface Science, 2004, 553, 155-167.
8. A. Curulli, A. Cusma, S. Kaciulis, G. Padeletti, L. Pandolfi, F. Valentini, M. Viticoli, “Immobilization of GOD and HRP enzymes on nanostructured substrates”, Surface and Interface Analysis, 2006, 38, 478-481.
9. S. Libertino, F. Giannazzo, V. Aiello, A. Scandurra, F. Sinatra, M. Renis, M. Fichera, “XPS and AFM Characterization of the Enzyme Glucose Oxidase Immobilized on SiO2 Surfaces”, Langmuir, 2008, 24, 1965-1972.
10. P. Smith, R. Krohn, G. Hermanson, A. Mallia, F. Gartner, M. Provenzano, E. Fujimoto, N. Goeke, B. Olson, D. Klenk, ”Measurement of protein using bicinchoninic acid”, Analytical Biochemistry, 1985, 150, 1, 76-85.
11. M. Fichera, S. Libertino, V. Aiello, A. Scandurra, F. Sinatra, M. Renis, S. Lombardo, “Glucose oxidase characterization for the fabrication of hybrid microelectronic devices”, Bioengineered and Bioinspired Systems III, Proceedings of the SPIE, 2007, 6592, 65920T.
12. V. Vojinovic, L. Bertin, J. Cabral, and L. Fonseca, “Horseradish Peroxidase Combined With Oxidase Enzymes a Valuable Bioanalytical Tool: Lactate Oxidase – A Case Study”, Engineering in Life Sciences, 2006, 6, 2, 181-186.

13. B. Sweryda-Krawiec, H. Devaraj, G. Jacob, J.J Hickman, “A New Interpretation of Serum Albumin Surface Passivation”, Langmuir, 2004, 20, 2054-2056.
14. D. Stenger, J. Georger, C. Dulcey, J.J. Hickman, A. Rudolph, T. Nielsen, S. McCort, J. Calve, “Coplanar Molecular Assemblies of Amino- and Perfluorinated Alkylsilanes: Characterization and Geometric Definition of Mammalian Cell Adhesion and Growth”, Journal of the American Chemical Society, 1992, 114, 8435-8442.
15. K. Lenghaus, J. Dale, C. Henderson, D. Henry, E. Loghin, and J.J. Hickman, “Enzymes as Ultrasensitive Probes for Protein Adsorption in Flow Systems”, Langmuir, 2003, 19, 5971-5974.
16. H. Rennke, M. Venkatachalam, “Chemical modification of horseradish peroxidase: Preparation and characterization of tracer enzymes with different isoelectric points”, Journal of Histochemistry and Cytochemistry, 1979, 27, 10, 1352-1353.

CHAPTER 2
ENGINEERING A TITANIUM AND POLYCAPROLACTONE CONSTRUCT FOR A BIOCOMPATIBLE INTERFACE BETWEEN THE BODY AND ARTIFICIAL LIMB

Introduction

Titanium is a commonly used material in dental and orthopedic applications because of its high mechanical properties, chemical stability, and biocompatibility[1]. Its excellent biocompatibility allows titanium implants to be directly anchored to bone or osseointegrated[2,3]. The conventional prosthetic replacement in amputees is a stump-socket design, which transfers force through the prosthetic to an external contact point on the patient. Such a design results in nonuniform distribution of pressure and can lead to pain, infection, and necrosis of the soft tissues at the point of contact[4,5].

It is believed that intraosseous transcutaneous amputation prostheses (ITAPs) can overcome these issues by directly attaching the implant to the skeleton through transcutaneous abutment[6]. Transcutaneous implants have been used clinically since the 1960s[7-9]. However, subsequent attempts to use similar implants in amputees have had limited success due to problems with loosening of the implant, mechanical failure, and infection[10]. This weak adhesion allows for invasion of bacteria at the tissue-implant interface.

It is believed that optimizing the attachment of the skin to the prosthetic will lead to clinically viable ITAPs[11]. Human skin is multifunctional and consequently has a complex architecture comprised of multiple layers with some indistinct boundaries. Skin acts as an active protective agent, or barrier, against traumas such as friction, impact, pressure, and shear stress. In addition many things have an effect on the properties of skin, including

the location of the skin on the body, the rate of application and duration of the stress, and the age of the skin[12].

In order to develop a clinically viable ITAP, the device must be mechanically strong, provide a tight seal at the biotic-abiotic interface, and take into account the complex properties of skin and other native tissues. In this study, a surface modified titanium construct was developed in order to build a surface that would allow for direct tissue adherence as well as scaffold adherence. Along with this construct, a novel Computer Aided Biology (CAB) Tool was used to fabricate a complex, three-dimensional (3D) polycaprolactone (PCL) scaffold on top of the titanium construct. PCL is well known for being a highly flexible biomaterial and was approved for use in surgical sutures over 30 years ago[13]. This study foused on characterizing these constructs and scaffolds, testing the adherence of the scaffolds to the titanium constructs, and examining different antibacterial agents to reduce bacteral invasion.

Materials and Methods

Description of the Computer Aided Biology Tool

The CAB Tool, which was previously known as the BioAssembly Tool or BAT[14,15], was developed to produce artificial constructs that would demonstrate properties of native tissue (microenvironment, 3D organization, and inter- cellular contact). The CAB Tool utilizes a computer-aided-design/computer-aided-manufacturing (CAD/CAM) approach to build heterogeneous tissue models. This system is a multi- head, through-nozzle deposition machine developed to conformably deposit biomaterials, cells, and co-factors on various supporting surfaces to create surrogate tissues and tentative platforms for experiments in cell biology and tissue engineering. The device contains: an XY

coordinate system with a stage; a number of Z-traveling deposition heads (currently up to 3), each of which is supplied with an individual controlling video camera; LED work area illumination; a fiber optic light source to illuminate the deposition area and cure photopolymers in-line; individual ferroelectric temperature controls for each deposition head; a water jacket temperature control for the stage; stainless steel and anodized work surfaces; and a piezoelectric humidifier.

Button Modification

Titanium buttons were generated from 2 mm thick, known-standard titanium foil (Sigma Aldrich, St. Louis, MO). A schematic of the buttons can be seen in Figure 8. Each button was machined such that there was a 2 mm thick round section with a 12.7 mm diameter, as well as a 6.35 mm tab that is 1 mm thick. All of the buttons were initially polished to a mirror finish using a coarse grit (36 grit) sandpaper followed by finer grit (400 and 800) sandpapers. The buttons were modified into four groups: (1) polished buttons, (2) polished buttons with holes, (3) acid etched buttons, and (4) acid etched buttons with holes. The buttons with holes (2 and 4) had a square array of 10 x 10 holes with 200 μm diameter, depth, and separation. The total 10x10 array of holes was 3.8 mm square. The acid etched buttons (3 and 4) were etched by immersing them in a 50:40 v/v mixture of 18% HCl and 48% H_2SO_4 at 60°C for 5 minutes. The buttons were then rinsed thoroughly in deionized water.

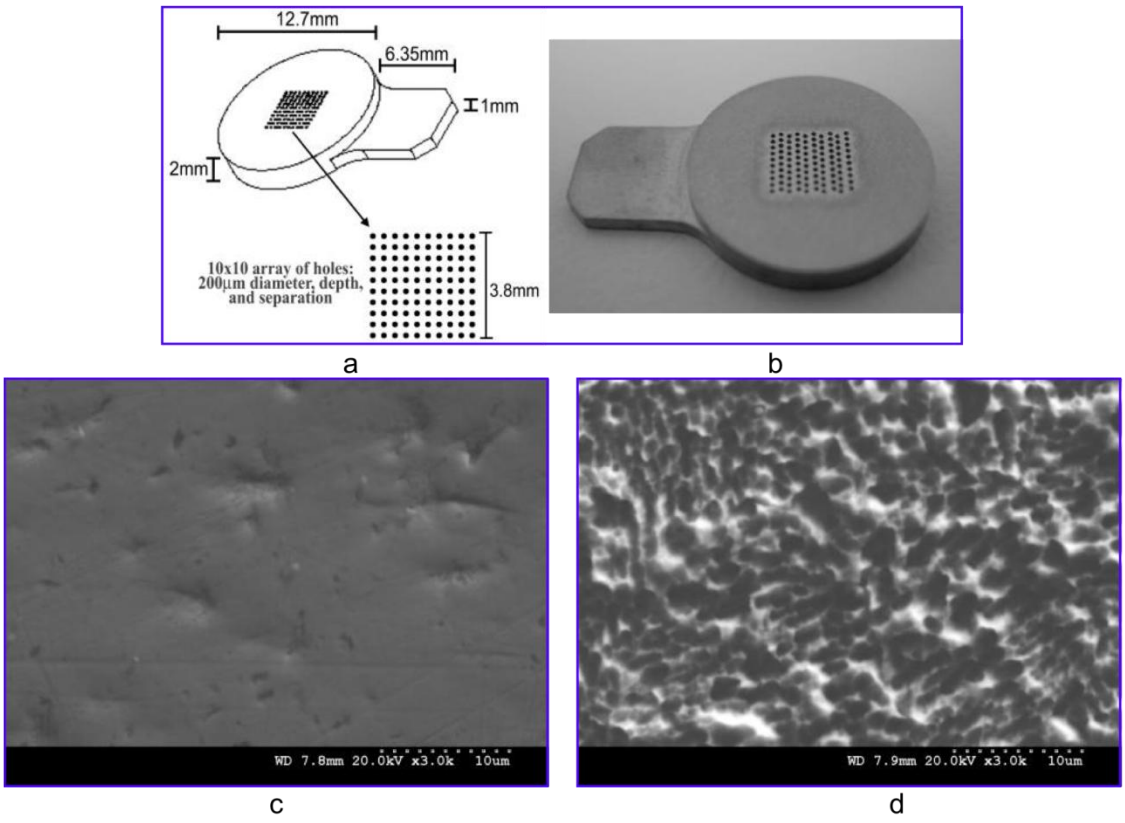

Figure 8. Titanium button design (a) A schematic drawing of the modified buttons (b) a representative picture of the buttons (c) SEM image of polished titanium button (d) SEM image of acid etched titanium button

Surface Roughness Measurements

The unmodified and modified titanium button surfaces were imaged using a Hitachi S3500N scanning electron microscope, with the accelerating voltage set to 20 kV. The surface roughness of the acid treated and plain titanium buttons with and without holes was measured with the help of a Zygo optical interferometer running Metro Pro software. The samples were all mounted on the stage, the z-stop position was calibrated, and the light intensity was adjusted to 85-90%. The objective lens focus was adjusted until the interference fringes could be observed and the stage roll and pitch were then adjusted until the fringes covered the entire surface to be measured. Next, the Metro Pro software

was used to capture the interference image and simultaneously reconstruct a pseudo-colored 3D profile of the surface. A region on the 3D profile was selected using the software crosshairs in order to automatically generate the average and root mean square (RMS) roughness values for that region. Three measurements were taken for the same surface and the values were averaged. The values were then plotted for the different surface treatments.

Preparing PCL for Printing

Polycaprolactone (PCL, molecular weight 80 kDa; Sigma Aldrich, St. Louis, MO) pellets were dissolved in glacial acetic acid (Sigma Aldrich, St. Louis, MO) at a concentration of 70% w/v. This concentration was found to be best for dispensing and ease of solvent evaporation, resulting in a solid structure. The mixture of PCL pellets and acetic acid was placed in a glass bottle with a sealed cap, and the solution was dissolved using a sonicator for 1-2 hours. After the PCL was fully dissolved, the solution was stirred with a spatula, backfilled into a 3-mL dispensing syringe (EFD, Providence, RI), closed with a stopper at the bottom and top of the syringe, and spun in a centrifuge at 2000 rpm for 5 minutes to remove air bubbles. This solution was then used for scaffold printing.

Printing PCL Scaffolds

The syringe was connected to an air pressure line for dispensing of the PCL solution. The ceramic dispensing tip used had an inner diameter of 100 μm and outer diameter of 150 μm. A pressure of 25 psi was used to push the PCL solution through the

ceramic tip orifice and deposit onto the target substrate. The printing speed (both XY stage and Z movement) of the dispensing pump was 2.5 mm/s. The speed is very important to the rate of evaporation of the acetic acid solvent, which therefore affected the creation of pores within the scaffold. A script (pen path) was created in AutoCAD and used to print the PCL scaffolds. The initial dispensing height was 50 μm and a lift of 25 μm between each layer. Scaffold designs were entered into the PathCAD program to generate porous constructs that were 5.4 mm x 5.4 mm. A single line of extrusion was used to generate the struts; thus, the designed strut thickness (width of the lines used to fabricate the PCL scaffold) was 100 μm. The input pore size (the open space in between the lines of PCL) was 300 μm. This scaffold was designed to be 130 μm tall, with a strut thickness of 100 μm. The printed scaffolds were measured, and the measured values were compared with the expected values. To bring the grids to a pH of 7.0, they were heated at 55°C for at least 6 hours, bathed in 90% ethanol for 30 minutes, and washed two times in PBS.

Strength of PCL Grids

Preliminary mechanical testing was conducted with a specially designed scaffold. This scaffold was fabricated to be similar to the scaffolds printed on the titanium buttons, with a height of 130 μm and a strut thickness of 100 μm. The scaffolds were longer (10 mm) and wider at one end. To test the tensile strength of the scaffold, the narrower end was fixed and the wider end was pulled until the scaffold broke. The force required to break the scaffolds was recorded, and the ultimate strength was calculated by dividing the force with the effective cross-sectional area (0.169 mm^2). On two separate days, 5

samples were printed and then stretched to determine the strength of the PCL grids.

Adhesion Testing

A tensiometer (Instron 3369, Instron Corp., Norwood, MA) was used to examine the peel off adhesion test for the PCL. A modified PCL grid was printed on the buttons for adhesion testing. These grids were printed such that there was a section of the grid hanging over the edge of the button. An aluminum jig was manufactured (in house) in order to attach the tensiometer to the PCL on the button, as can be seen in Figure 9. This jig had one plate with a circular groove in it where the buttons were placed and another aluminum plate was placed over it and screwed into place to secure the button. This section was then attached to one end of the tensile tester. The free end of the printed PCL was adhered to another plate with glue, which was then attached to the other testing end of the tensile tester. The crossheads were moved in opposite directions producing a tensile force on the PCL-titanium interface. The crosshead speed was set at 3 mm/min. The test was carried out until either the PCL peeled off from the titanium substrate or broke into two pieces. The software generated values for the break load, maximum load, and the maximum displacement. The stress (MPa) vs. strain curves were calculated, and the adhesion strength (MPa) for each surface treatment was assigned the value of the maximum stress from the corresponding curve. On two separate days, 3 measurements were taken for each surface treatment and the values were then averaged and the standard deviations were calculated and plotted.

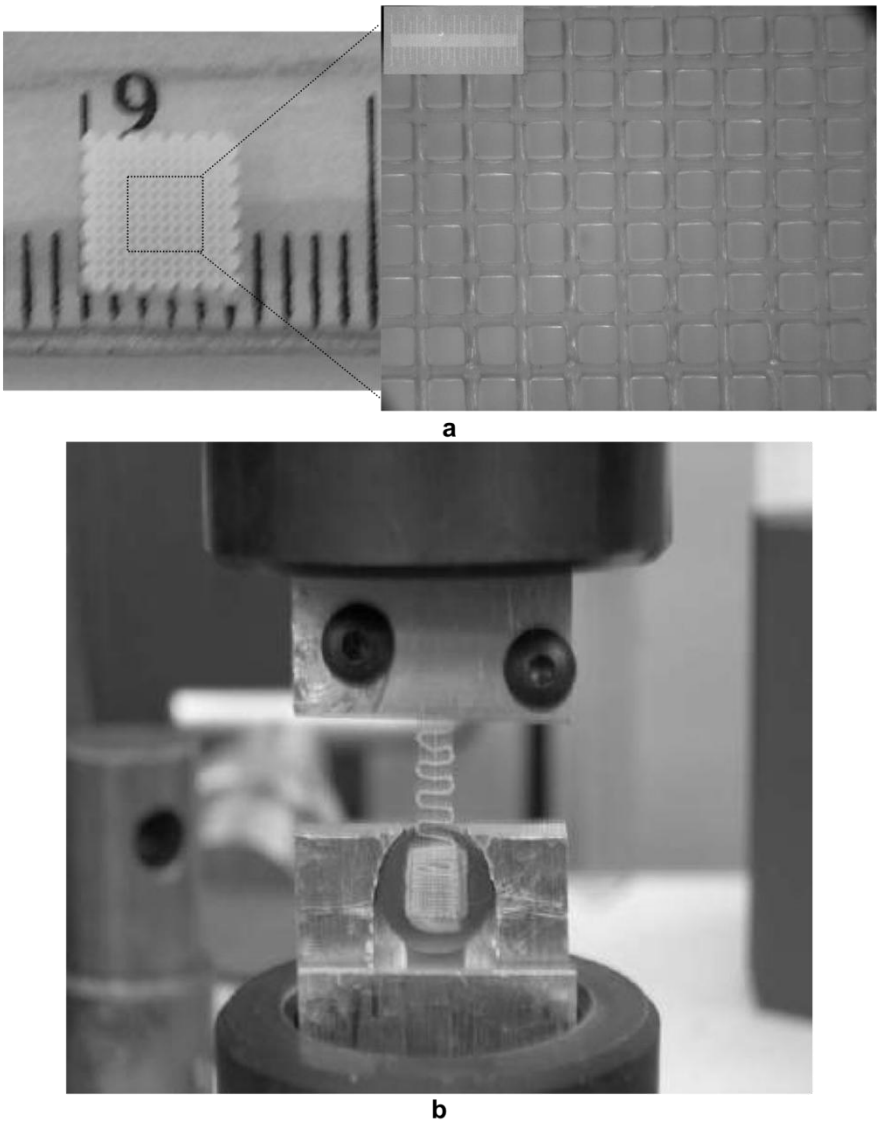

Figure 9. Printed PCL grid (a) A representative picture of the printed PCL grid (units in mm) (b) Tensile strength testing of PCL grid

Cell Culture on PCL

Solutions of PCL alone and 70% PCL in acetic acid were extruded into 6-well tissue culture polystyrene (TCPS) plates at a volume of 100 μL. Each extrusion was neutralized and sterilized by heating at 55°C for 6 hours, bathing in 90% ethanol for 30 minutes, and then rinsing twice with PBS. Human dermal fibroblast cells (Hs68; ATCC, Manassas, VA) were cultured in media containing 90% Dulbecco's Modified Eagle's

Medium (DMEM; ATCC, Manassas, Va) + 10% Fetal Bovine Serum (ATCC, Manassas, VA) with 1% penicillin/streptomycin (Sigma Aldrich, St. Louis, MO) according to the ATCC cell culture protocol. When the cells reached confluence, they were seeded at a concentration of 10^5 cells/mL onto the PCL, 70% PCL in acetic acid, and plain TCPS. After 1 hour, the constructs were rinsed with PBS and cell media was added. After 3 days, the viability of the cells was assessed using a fluorescent live/dead assay (Invitrogen, Carlsbad, CA). Cell viability was assessed twice with a sample size of 5 for each group.

Assessing Cell Viability

To assess the viability of the constructs, a staining solution containing calcien AM and ethidium homodimer in divalent-cation free PBS (DCF-PBS) was prepared following the instructions included with the kit. The constructs were washed with DCF-PBS and then bathed in the staining solution for 30 minutes at room temperature, and protected from light. The constructs were then washed 2 times for 15 minutes with DCF-PBS and imaged within 1 hour after staining by using an epifluorescent microscope to image the live (excitation, 488 nm; emission 530 nm) and dead (excitation, 528-553 nm; emission, 580 nm) cell fluorescence. The total number of cells were counted within 5 fields of view. Cells with homogeneous bright green staining throughout the cell were counted as live, and cells with bright red staining were counted as dead. Percentage viability was calculated as the number of live cells divided by the total number of cells counted.

Preparing Antibacterial Samples

Type I collagen (Col) and hyaluronic acid (HA) solutions were mixed with one of three antibacterial materials, either silver nanoparticles (Ag; Sigma Aldrich, St. Louis, MO), Titanium dioxide anatase (TiO_2; Sigma Aldrich, St. Louis, MO), or chlorhexadine diacetate (ChD; Sigma Aldrich, St. Louis, MO). A 3.0 mg/mL collagen solution was prepared as previously described[14]. Briefly, purified rat-tail collagen type I (BD Biosciences, Bedford, MA) was mixed with Dulbecco's Modified Eagle's Medium (DMEM) and brought to a pH of 7.0-7.4 by the addition of 1 M NaOH. A solution of HA was prepared from an Extracel Hydrogel kit (Glycosan Biosystems, Inc., Salt Lake City, UT) by following the given protocol. After the Col or HA solution was prepared, an antibacterial agent was mixed into the solution at 1-10% w/w by gently pipetting. Next, 100 μL of the solution was placed in a 6 well plate and allowed to fully polymerize at 37°C for 1 hour.

Antibacterial Assay

Staphylococcus aureus (ATCC, Manassas, VA) was grown in Caso broth (casein-peptone soymeal-peptone broth) overnight at 37°C in a water bath. The antibacterial samples (described above) were incubated at 37°C for 1 hour in the Caso broth solution containing *S. aureus*. Aliquots of broth were obtained from each group. The aliquots were stained with Crystal Violet for 15 minutes, and an acetic acid solution was added to solubolize the stained bacteria in the broth. The bacteria were then quantified using a spectrophotometer at 630 nm. These experiments were performed on two separate days with a sample size of 5 for each group.

Statistics

In order to assess the differences between treatments, each experiment was carried out as described in their corresponding sections. The measured values were then examined using a Student's T test. A difference in values was only labeled as a "significant" difference if the p value was less than 0.05.

Results

Button Modification

As shown in Figure 8, buttons were machined from 2 mm thick titanium foil such that there was a 2 mm thick round section with a 12.7 mm diameter and a 6.35 mm long tab that was 1 mm thick. Half of the buttons had a 10 x 10 array of holes that were 200 μm in diameter, depth, and separation. All of the buttons were polished to a mirror finish. Then, half of the holed buttons and half of the non-holed buttons were acid etched to increase surface roughness.

Surface Roughness

Figure 8 illustrates the SEM images of the polished and acid etched buttons, respectively. Using a Zygo optical interferometer, the RMS surface roughness was measured for the button groups: polished without holes (P), polished with holes (H), aid etched without holes (AE), and acid etched with holes (AEH). These results can be seen in Figure 10a. No significant difference was observed in the surface roughness of the two polished groups (P and H). A significant increase ($p < 0.05$) was noted in the surface roughness of the acid etched groups (AE and AEH) when compared to the polished buttons.

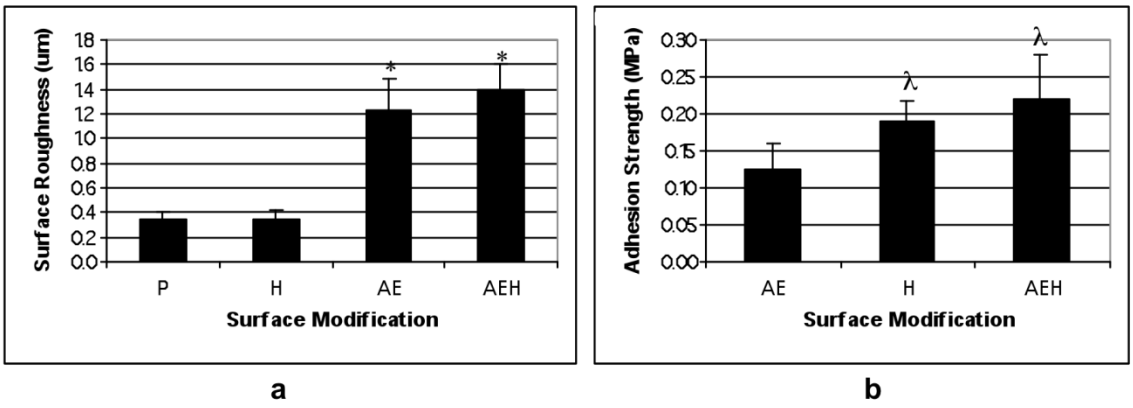

Figure 10. Surface roughness and adhesive strength for button modifications (a) Root mean square roughness was measured using an interferometer for polished (P) buttons, buttons with holes (H), acid etched buttons (AE) and acid etched buttons with holes (AEH) (b) Adhesion strengths were measured for the AE, H, and AEH groups. * indicates a significant increase in surface roughness of buttons as compared with polished buttons ($p < 0.05$). λ indicates a significant increase in strength of buttons as compared to acid etched buttons ($p < 0.08$)

Precision of Printed PCL Grids

Porous scaffolds are sometimes desired to provide an area for cells to migrate and proliferate or for controlled release of chemicals[16]. The CAB tool can print complex 3D scaffolds with different designs in terms of overall shape, dimension, and pore size. In order to test the accuracy of the CAB tool using 70% PCL, a 5.4 mm x 5.4 mm x 1.5 mm (LxWxH) scaffold was fabricated. Figure 9 demonstrates a representative scaffold that was printed using the CAB tool. This figure shows that the struts and pores within the scaffold are uniform and evenly spaced. The printed scaffolds were measured and the measured values were compared with the expected values. A single, non-overlapping line was extruded in order to generate each strut within the scaffolds. Since the dispensing tip used had an inner diameter of 100 μm, the expected strut size was 100 μm. The pore size (the open space in between the lines of PCL) that was programmed into the script was 300 μm. The measured strut size was 65 ± 12 μm; and the measured pore size was 315 ±

10 μm. The overall porosity of the scaffolds was 54 ± 1%.

Tensile Strength of PCL Grids

To demonstrate that the printing process of the CAB tool does not significantly alter the strength of the printed PCL, a special scaffold design was entered into the PathCAD software. These scaffolds were able to hold between 4-8 pounds before ultimately breaking. Using the effective cross sectional area of 0.169 mm^2, the ultimate strength varied from 24 to 40 MPa with an average of 29.62 MPa.

Adhesion Testing

When PCL was printed on top of the smooth titanium buttons, the PCL peeled off of the buttons upon drying. When the Titanium buttons were either acid etched or holes were added to the button surface, the PCL would remain on the Titanium button. The different surface modifications were examined to determine which provided the best adhesion between the PCL and the button. The average adhesive strengths for the acid etched buttons (AE), polished buttons with holes (H), and acid etched buttons with holes (AEH) can be seen in Figure 10b. Buttons that were acid etched, had an average adhesive strength of 0.13 MPa. When holes were added to the buttons, there was a significant increase ($p < 0.05$) in the adhesive strength as compared with acid etched buttons with no holes. However, while there was a slight increase in the average adhesive strength, a significant difference was not noted between the holed buttons that were acid etched and the holed buttons that were polished. Thus, the addition of holes gave the desired result of a significant increase in adhesive strength.

Cell Viability

To verify that the preparation of 70% PCL in acetic acid would not effect the viability of cells, human dermal fibroblasts were seeded onto sterile, neutralized 70% PCL in acetic acid, PCL alone, and on TCPS. There was a significant decrease ($p < 0.05$) in the viability of cells seeded on the 70% PCL (10% decrease) or plain PCL (15% decrease) as compared with cells seeded on TCPS. When the number of cells was counted on the three test surfaces, there was a significant increase (53%; $p < 0.05$) in the number of cells seen on TCPS as compared with either of the PCL surfaces.

Antibacterial Assay

Initially, examination was done using different antibacterial agents (Silver nanoparticles [Ag] and Titanium Dioxide Anatase [TiO_2]) within the PCL or coating the PCL. However, a significant decrease in the viable bacteria when using these methods was not observed. Based on these results, the antibacterial activity of different antibacterial agents (Ag, TiO_2, and Chlorhexidine Diacetate [ChD]) embedded in natural biomaterials, type I Collagen (Col) or Hyaluronic Acid (HA) were examined. Figure 11a indicates the absorbance readings by spectrophotometer. No significant difference was observed in the viable bacteria seen on either Col or HA alone when compared with the bacteria broth. Figure 11b demonstrates the percentage of bacteria seen in the treatment groups using bacteria in broth as the standard number of bacteria in broth at the same time point. A significant decrease ($p < 0.05$) in bacteria was seen when 10% w/w TiO_2 was added to either Col or HA. Also, a significant decrease ($p < 0.05$) in bacteria was

observed when 10% w/w ChD was added to the HA. This decrease was not significant when the ChD was added to the Col. A significant decrease in bacteria was noted in the treatment groups using HA with varying concentrations of either ChD or TiO_2 (1% - 5% w/w). No significant decrease in the bacteria was observed when TiO_2 was used. However, there was a significant decrease in bacteria when any concentration of ChD was added to the HA.

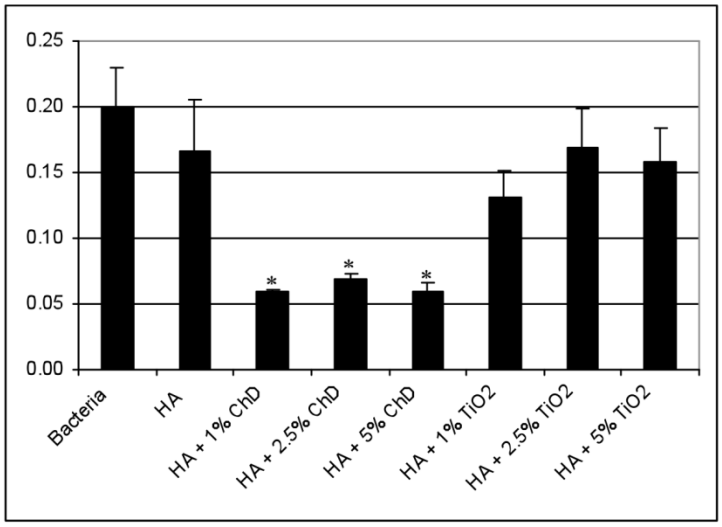

a

Treatment	Percent
None	100.00
HA Alone	82.92
HA + 1% ChD	**29.67**
HA + 2.5% ChD	**34.17**
HA + 5% ChD	**29.77**
HA + 1% TiO_2	65.63
HA + 2.5% TiO_2	84.12
HA + 5% TiO_2	79.22

b

Figure 11. Average viable bacteria as seen by interferometer (a) Viable bacteria as seen with various antibacterial agents chlorhexidine diacetate (ChD), titanium dioxide (TiO2) mixed in with the hyaluronic acid (HA). * indicates a significant decrease in bacterial viability as compared with HA alone ($p < 0.05$). (b) The percentage of bacteria seen in treatment groups using bacteria in broth as the standard number of bacteria in broth at the same time point. A significant decrease from the non-treatment group was only seen in the bold groups ($p < 0.05$)

Discussion

Due to the nonuniform distribution of pressure in conventional stump-socket prosthetic replacements, amputees have problems with pain, infection, and necrosis of the soft tissues at the point of contact[4,5]. ITAPs would allow for direct anchoring to the bone, thus potentially overcoming these problems. However, limited success has been seen in such devices in amputees[6-10]. It is believed that clinically viable ITAPs may be achieved by creating a construct that has tight adherence of the overlying scaffold[11]. This study characterizes the fabrication of a PCL scaffold on top of a surface modified titanium construct with a primary focus on creating a tight adherence.

When using the CAB Tool to generate spatially organized 3D PCL constructs, it was concluded that a 70% solution of PCL in acetic acid was the best concentration to use for consistency in printing. Porous scaffolds are often required for biomedical applications, because the pores provide an area for cells to migrate and proliferate[16]. For this study, porous scaffolds were fabricated using a 100 μm ceramic with programmed pores of 300 μm. The resulting scaffolds had an average strut width of 65 ± 12 μm and a pore size of 315 ± 10 μm. The resulting porosity was 54 ± 1%.

Previous research has demonstrated that PCL has an average ultimate strength of 29 – 42 MPa[17,18]. The PCL constructs printed in this study had an average tensile strength of 29.62 MPa. This falls within the range of previously reported values[17]. The tensile strength of human skin has been measured as 17 – 21 MPa[12]. Thus, the scaffolds produced in this study have shown great promise in their utility for alternative skin in prosthetic devices since their strength is similar to that of natural skin.

When PCL was printed on top of smooth titanium buttons, the PCL peeled off of

the buttons upon drying. It has been demonstrated that the addition of surface roughness to titanium surfaces increased the osseo-integration of the implanted construct[19]. Thus, when titanium buttons were either acid etched or the surface was machined with an array of holes, the PCL was able to adhere to the titanium. Buttons that were acid etched, had an average adhesive strength of 0.13 MPa. A significant increase in the adhesive strength was observed when an array of holes was added to the surface of the titanium. The adhesive strength increased to 0.19 MPa for buttons with only holes (H) and to 0.22 MPa for buttons with both holes and acid etching (AEH). Thus, the addition of the array of holes does significantly increase the adhesive ability of Titanium.

Orr et al., defined an adhesive as a material that exhibited an adhesive strength of greater than 0.1 MPa, and materials that had an adhesive strength lower than this were sealants[20]. With an adhesive strength of 0.22 MPa, printing a PCL grid on acid etched and machined (AEH) titanium is an adhesive, and can be effectively treated as a bio-concrete. Sarasam and Madihally demonstrated that PCL dissolved in acetic acid could be used in polymeric blends in biomedical applications[21]. In this study, it was noted that when the 70% PCL in acetic acid constructs were dried at 55°C and then bathed in 90% EtOH for 30 minutes, the constructs were neutralized, and thus compatible with viable cells. When the viability of cells was examined, there was a slight (10%) difference in the viability of cells seeded onto 70% PCL as compared with TCPS. Significantly fewer (53%) cells were noted on the 70% PCL after three days in culture. These results demonstrated that the 70% PCL does not have an adverse effect on the viability of cells.

When an antibacterial agent was added to the PCL or placed on the titanium button, there was no significant decrease in the number of viable bacteria when compared to

bacteria in the culture. However, when an antibacterial agent was added to type I collagen or hyaluronic acid, there was a significant decrease. Lower concentrations of antibacterial agents were tested, and with as low a concentration as 1% (w/w) chlorhexidine diacetate mixed in HA, there was a significant decrease in the viable bacteria. It was also noted that the chlorhexidine diacetate was more effective at low concentrations in HA than it was in the type I collagen. Thus, by adding an antibacterial agent within HA, bacterial invasion can be greatly decreased.

Conclusion

The results demonstrate that by not only adding roughness, but by adding surface features such as holes, the adhesive strength of titanium can be greatly increased. Also, the fabrication of a porous PCL scaffold on top of the titanium has tensile strengths similar to that of natural skin. With the addition of a coating of HA containing an antibacterial agent, such as chlorhexidine diacetate, the bacterial resistance of the titanium and PCL construct will be greatly increased. It will greatly advance the application of ITAPs in the medical field if the engineered titanium and PCL construct successfully promotes effective *in vivo* adhesion between the titanium-epithelium interface, thus preventing infection of the skin and underlying tissue adjacent to prosthetic implants.

We would like to gratefully acknowledge the collaboration with Dr Tithi Duttaroy, Dr Cindy Smith, and Dr Ken Church at nScrypt Inc. for providing all their help with this project.

References

1. Pohler, O.E. Unalloyed titanium for implants in bone surgery. Injury 31, Supplement 4, 7, pages D7-D13, 2000.
2. Bränemark, P.I., Hansson, B.O., Adell, R., Breine, U., Lindström, J., Hallen, O., and Ohman, A. Osseointegrated implants in the treatment of the edentulous jaw: Experience from a 10-year period. Scandinavian Journal of Plastic and Reconstructive Surgery Supplement 6, 1, 1977.
3. Albrektsson, T., Bränemark, P.I., Hansson, H.A., and Lindström, J. Osseointegrated titanium implants: Requirements for ensuring along-lasting, direct bone-to-implant anchorage in man. Acta Orthopaedica Scandinavica 52, 155, 1981.
4. Dudek, N.L., Marks, M.B., and Marshall, S.C. Skin problems in an amputee clinic. American Journal of Physical Medicine and Rehabilitation 85, 424, 2006.
5. Levy, S.W. Amputees: skin problems and prostheses. Cutis 55 297, 1995.
6. Pendegrass, C.J., Gordon, D., Middleton, C.A., Sun, S.N., and Blunn, G.W. Sealing the skin barrier around transcutaneous implants: in vitro study of keratinocyte proliferation and adhesion in response to surface modifications of titanium alloy. The Journal of Bone and Joint Surgery. British Volume 90, 114, 2008.
7. Bränemark, P.I., Breine, U., Adell, R., and Breine, U. Intraosseous anchorage of dental prostheses. Scandinavian Journal of Plastic and Reconstructive Surgery 3, 81, 1969.
8. Bränemark, P .I. T ooth replacement by oral endoprostheses: clinical aspects. The International Journal of Oral Implantology 5, 27, 1988.
9. Bränemark, R., Branemark, P.I., Rydevik, B., and Myers, R.R.. Osseointegration in skeletal reconstruction and rehabilitation: a review. Journal of Rehabilitation Research and Development 38, 175, 2001.
10. Sullivan, J., Uden, M., Robinson, K.P., and Sooriakumaran, S. Rehabilitation of the trans-femoral amputee with an osseointegrated prosthesis: the United Kingdom experience. Prosthetics and Orthotics International 27, 114, 2003.
11. Pendegrass, C.J., Goodship, A.E., Price, J.S., and Blunn, G.W. Nature's answer to breaching the skin barrier: an innovative development for amputees. Journal of Anatomy 209, 59, 2006.
12. Edwards, C. and Marks, R. Evaluation of biomechanical properties of human skin. Clinical Dermatology 13, 375, 1995.
13. Bezwada, R.S., Jamiolkowski, D.D., Lee, I.Y., Agarwal, V., Persivale, J., Trenka-Benthin, S., Emeta, M., Suryadevara, J., Yang, A., and Liu, S. Monocryl suture, a new ultra-pliable absorbable monofilament suture. Biomaterials, 16, 1141, 1995.
14. Smith, C.M., Stone, A.L., Parkhill, R.L., Stewart, R.L., Simpkins, M.W., Kachurin, A.M., Warren, W.L., and Williams, S.K. Three-dimensional bioassembly tool for generating viable tissue-engineered constructs. Tissue Engineering 10, 1566, 2004.
15. Smith, C.M., Christian, J.J., Warren, W.L., and Williams, S.K. Characterizing environmental factors that impact the viability of tissue-engineered constructs fabricated by a direct-write bioassembly tool. Tissue Engineering 13, 373, 2007.
16. Leong, K.F., Phua, K.K., Chua, C.K., Du, Z.H., and Teo, K.O. Fabrication of porous polymeric matrix drug delivery devices using the selective laser sintering

technique. Proceedings of the Institution of Mechanical Engineers. Part H 215, 191, 2001.
17. Hutmacher, D.W., Schantz, T., Zein, I., Ng, K.W., Teoh, S.H., and Tan, K.C. Mechanical properties and cell cultural response of polycaprolactone scaffolds designed and fabricated via fused deposition modeling. Journal of Biomedical Materials Research, 55, 203, 2001.
18. Matzinos, P., Tserki, V., Gianikouris, C., Pavlidou, E., and Pabayiotou, C. Processing and characterization of LDPE/starch/PCL blends. European Polymer Journal, 38, 1713, 2002.
19. Le Guéhennec, L., Soueidan, A., Layrolle, P., and Amouriq, Y. Surface treatments of titanium dental implants for rapid osseointegration. Dental Materials, 23, 844, 2007.
20. Orr, T.E., Patel, A.M., Wong, B., Hatzigiannis, G.P., Minas, T., and Spector, M. Attachment of periosteal grafts to articular cartilage with fibrin sealant. Journal of Biomedical Materials Research. 44, 308, 1999.
21. Sarasam, S. and Madihally, S.V. Characterization of chitosan–polycaprolactone blends for tissue engineering applications. Biomaterials, 26, 5500, 2005.

CHAPTER 3
SKELETAL MUSCLE TISSUE ENGINEERING ON BIOMEMS DEVICES

Introduction

The integration of biological components with artificial devices is very important for creating bio-hybrid devices for a variety of functions and applications. Skeletal muscle can be integrated with BioMEMS devices and can be useful in a number of applications, including biorobotics, bioprostheses, tissue replacement, physiological and pharmacological studies and diseased models.

Previously fetal rat muscle cells harvested from E18 rat embryos were able to form functional myotubes on a synthetic self assembled monolayer substrate (DETA) and its subsequent integration with silicon based cantilever structures[1]. A completely defined, serum-free medium to culture the cells was also developed. Immunocytochemistry and electrophysiology studies were able to show the formation of functional myotubes on both surfaces. The detailed protocol for the cantilever fabrication, surface functionalization and cell culture are documented in Das, 2007[2].

After having shown the integration of the myotubes with the cantilever devices, our group was also able to quantitatively measure the contractile forces exerted by the functional myotubes using a novel AFM detection setup utilizing a laser, photodiode and a X-Y stage using micromotors[3]. In the study a 2V bipolar pulse with pulse duration of 40 ms and frequency of 1 Hz was applied to the myotubes cultured on the cantilevers to show the rhythmic contraction of the myotubes. Applying a higher frequency pulse resulted in tetanic conditions.

To evaluate the surface cues needed for skeletal muscle to differentiate, vitronectin was patterned on the DETA substrates and C2C12 cells were cultured on the patterns[4]. Vitronectin was also patterned on top of commercial, substrate embedded microelectrodes. The cells differentiated and formed functional myotubes, which were evaluated using myosin heavy chain staining. The novelty of this study was that instead of adding vitronectin to the growth and differentiation medium, the authors found that the surface bound vitronectin worked better[4].

Ishibashi et al[5] studied the electrical stimulation of C2C12 cells on a porous alumina substrate sealed by PDMS. They were selectively able to block certain areas of the substrate using air bubbles, so that the electrical field could not be applied to that area. The stimulation of the C2C12 myotubes was visualized by a Fluo-4 dye, which showed the calcium transients in response to the externally applied electrical stimulus.

To develop skeletal muscle fibers for tissue engineered grafts, Zhao et al[6] cultured C2C12 myoblasts on a PDMS polymer microchip with linearly aligned microgrooves. The myoblasts attached, grew and differentiated to form myotubes and also formed 3D multi-layered structures. They also found that the deeper grooves worked better in aiding the alignment of the cells. Cimetta et al[7] also cultured C2C12 cells and rat neonatal rat cardiomyocytes on polyacrylamide based hydrogels modified by micro-contact printing of extracellular matrix proteins.

Skeletal muscle cultures respond to chemical cues in the surrounding milieu. However, Zhao[8] studied skeletal myogenesis using electrical stimulation cues. They fabricated a microelectrode array, cultured C2C12 cells on the surface, and applied a low intensity (500 mV), but high frequency (1000 kHz), signal to the electrodes. The cells

proliferated and reached confluency. They also differentiated into functional myotubes as evidenced by the MHC and actin filament staining.

Another cue for muscle differentiation using external mechanical stimulation was shown in a study by Vandenburgh et al[9]. In this study primary human skeletal muscle cells were used. The cells were grown in a silicone mold with end attachment sites. Similar to mechanical loading *in vivo*, the cells were then attached to posts of a mechanical stimulator setup, which mechanically moved the posts, providing tension to the muscle cells. This repetitive stretching/relaxation increased the muscle elasticity, mean myofiber diameter and myofiber area.

Skeletal muscle on BioMEMS can also be used as a bio micro-actuator. In the first study Dennis et al[10] designed and built a swimming robot actuated by two explanted frog semitendinosus muscles. The robot performed basic swimming maneuvers in an extracellular ringer solution and remained active for 42 hours. Montemagno et al[11] built a micromechanical device operated by muscle bundles starting from muscle cells. The muscle cells were cultured onto a thin gold bridge between a free standing cantilever and a post. This provided a novel way to characterize the properties of muscle bundles. They also created an autonomous mechanical object which moved on a surface in response to muscle contraction fuelled by glucose.

In this study, embryonic rat skeletal muscle cells from E18 embryos and spinal cord motoneurons from E15 embryos were co-cultured on a patterned, silicon based microcantilever device. The culture was maintained in the defined medium[2]. After 10-12 days in culture, the co-culture system was interrogated with an AFM detection system. The muscle contraction dynamics on application of a defined external electric field

stimulation was recorded. The system was also interrogated with the excitatory neurotransmitter glutamate to show the existence of a neuro-muscular junction.

Materials and Methods

Surface modification and characterization of cantilever devices

The cantilever devices were cleaned by soaking them in 3:1 v/v solution of concentrated sulfuric acid and hydrogen peroxide (piranha solution) and raising the temperature to 120°C for 10 minutes. The devices were subsequently rinsed thoroughly with deionized water and dried in an oven overnight. The devices were then coated with a PEG alkylsilane 2-[Methoxypoly(ethyleneoxy)propyl]trimethoxysilane for 30 minutes according to a previously established protocol[2]. The PEG modified surfaces were then patterned using deep UV laser ablation with a specific photomask, which ablated the PEG from the cantilever surfaces and also created somal adhesion sites for the motoneurons. The ablation was done for 40 seconds, and after ablation the surfaces were then backfilled with DETA (3-Trimethoxysilyl propyl) diethylenetriamine alkylsilane according to a previously established protocol[2]. Glass coverslips (22x22 mm) were used as controls and were subsequently characterized with contact angle goniometry and XPS.

Cell culture and electrical characterization of muscle-motoneuron coculture

Motoneurons and hind limb skeletal muscle cells were harvested from day 15 and day 18 (E18) rat embryos, respectively, obtained from pregnant Sprague-Dawley rats. A cell count was performed and the motoneurons and muscle cells were each plated at a density of 200 cells/mm^2 on the cantilevers using a PDMS cell separation chamber of our own

design. The cells were imaged on day 10. Figure 12 indicates a representative phase picture of a cantilever which shows a number of myotubes formed that span the entire length of the cantilever. Similar myotube structures were observed on other cantilevers as well. The motoneurons were not visible because they lie on the silicon substrate.

Initially it was necessary to determine if the myotubes were functional and contractile. The cantilevers were placed in a field stimulation chamber filled with extracellular media and an electrical stimulation was applied to the cells using micro-electrodes. The field stimulation pulse was a bipolar pulse with an amplitude of ± 2 V, pulse duration of 40 ms and frequency of 1 Hz. Figure 13 shows the oscilloscope readings from the photodiode due to the contraction of the myotube. It also indicates the synchronization of the response (upper panel) with the trigger stimulus (lower panel).

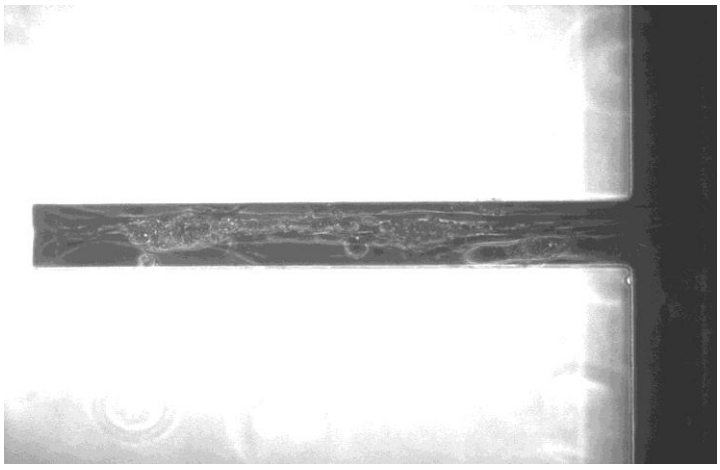

Figure 12. Myotube formation on patterned cantilevers (day 10, 20x magnification)

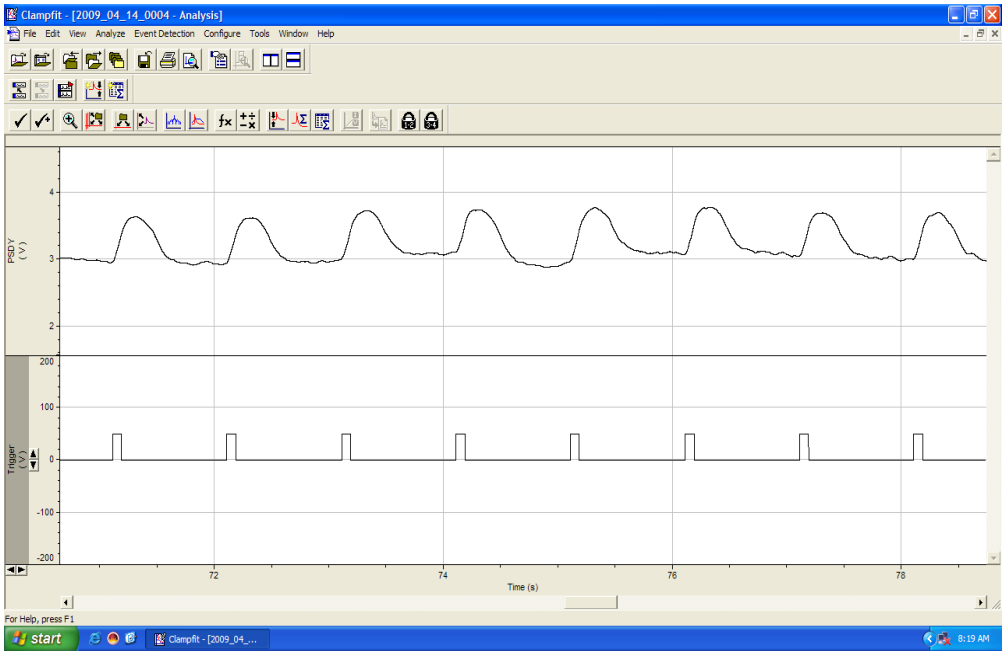

Figure 13. Field stimulation of the co-culture showing contractile behavior of the muscle

Administration of extracellular glutamate to motoneuron muscle coculture on cantilevers

The next step was to interrogate this system with glutamate, which is an excitatory neurotransmitter. The experiment was performed on day 14. The field stimulation was switched off and a single dose (30 μL) of 50 mM glutamate was added to 2 mL of the media 30 seconds after the AFM recording was started. Figure 14 shows the oscilloscope readings before and after the glutamate administration. Contractile behavior of the myotubes was observed after the administration, which was aperiodic in nature (upper panel). The lower panel shows the field stimulation which was turned off during the experiment. The recording was performed for over 3 minutes. The glutamate containing media was then replaced with fresh media and no further contractions were observed.

As a control experiment, another cantilever device was cultured with only muscle cells and the cells were tested for their contractility using the field stimulation. Again a single dose of 50 mM glutamate was administered into media 45 seconds after the recording was started. Figure 15 shows the oscilloscope readings. No contractile behavior of the myotubes was observed.

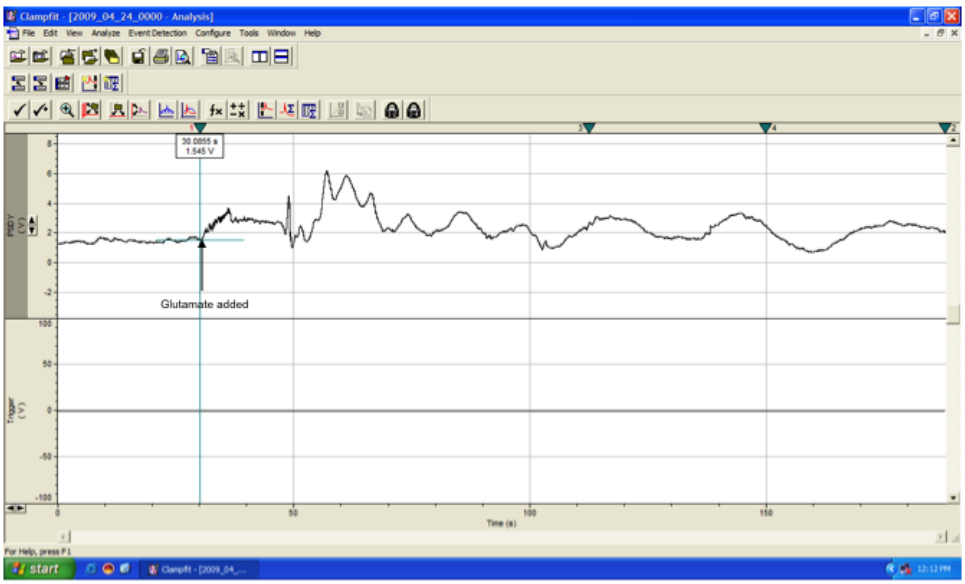

Figure 14. Glutamate administration to muscle-motoneuron coculture

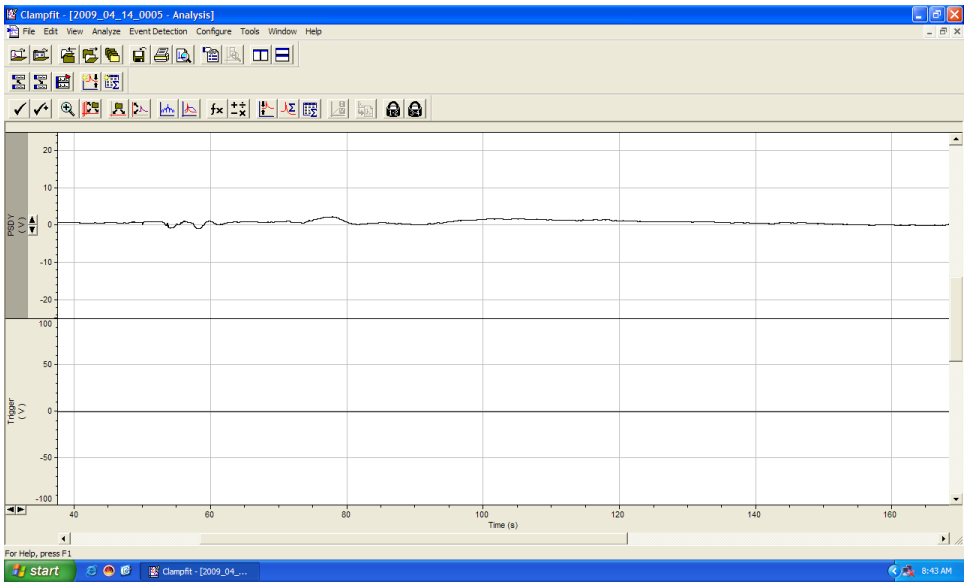

Figure 15. Glutamate administration to pure muscle culture

Conclusion

A novel silicon based micro-cantilever device was used to create a platform for studying skeletal muscle tissue engineering. Embryonic rat motoneurons and hind limb muscle were cocultured on the device and the system was probed for the formation of functional neuro-muscular junctions by using the excitatory neurotransmitter glutamate. Future studies will continue to probe for this functional aspect and the applications include studying diseased models and high throughput drug screening.

References

1. Mainak Das, Cassie Gregory, Peter Molnar, Lisa Riedel, Kerry Wilson, James J. Hickman, "A defined system to allow skeletal muscle differentiation and subsequent integration with silicon microstructures", Biomaterials 2006, 27, 4374-4380.
2. Mainak Das, Kerry Wilson, Peter Molnar, James Hickman, "Differentiation of skeletal muscle and integration of myotubes with silicon microstructures using serum-free medium and a synthetic silane substrate", Nature Protocols, 2007, 2, 7, 1795-1801.
3. Kerry Wilson, Peter Molnar, James Hickman, "Integration of functional myotubes with a Bio-MEMS device for non-invasive interrogation", Lab on a Chip, 2007, 7, 920-922.
4. Peter Molnar, Weishi Wang, Anupama Natarajan, John W Rumsey, James J Hickman, "Photolithographic patterning of C2C12 myotubes using vitronectin as growth substrate in serum-free medium", Biotechnology Progress, 2007, 23, 265-268.
5. Takeshi Ishibashi, Yu Hoshino, Hirokazu Kaji, Makato Kanzaki, Masaaki Sato, Matsuhiko Nishizawa, "Localized electrical stimulation to C2C12 myotubes cultured on a porous membrane-based substrate", Biomedical Microdevices, 2009, 11, 413-419.
6. Yi Zhao, Hansong Zeng, Jin Nam, Sudha Agarwal, „Fabrication of skeletal muscle constructs by topographic activation of cell alignment", Biotechnology and Bioengineering, 2009, 102, 2, 624-631.
7. Elisa Cimetta, Sara Pizzato, Sveva Bollini, Elena Serena, Paolo de Coppi, Nicola Elvassore, "Production of arrays of cardiac and skeletal muscle myofibers by micropatterning techniques on a soft substrate", Biomedical Microdevices, 2009, 11, 389-400.
8. Yi Zhao, "Investigating electric field-affected skeletal myogenesis using a microfabricated electrode array", Sensors and Actuators A: Physical, 2008.
9. Courtney Powell, Beth Smiley, John Mills, Herman Vandenburgh, "Mechanical stimulation improves tissue-engineered human skeletal muscle", American Journal of Physiology Cell Physiology, 2002, 283, 1557-1565.
10. Hugh Herr, Robert Dennis, "A swimming robot actuated by living muscle tissue", Journal of Neuroengineering Rehabilitation, 2004, 1, 1-6.
11. Jianzhong Xi, Jacob Schimdt, Carlo Montemagno, "Self-assembled microdevices driven by muscle", Nature Materials, 2005, 4, 180-184.

CONCLUSION

The work in this thesis involves the study of the interactions of proteins, cells and tissues with biomaterials. The first part addresses the question of protein adsorption on surfaces. Glucose oxidase and horseradish peroxidase were adsorbed to a fluorinated and glass surface. The concentration dependent adsorption characteristics were quantified using X-ray photoelectron spectroscopy and micro-BCA biochemical assay. The data obtained was then fitted with a simple Langmuir adsorption model equation. The affinity/binding constants of the proteins to the surfaces was also derived. These values were then compared with each other.

In the second part, tissue interactions with biomaterials were observed. A poly-caprolactone based tissue-engineering construct was printed on a titanium substrate. The optical and mechanical characteristics were evaluated. Human fibroblast cells were then seeded on the construct and their viability was assessed. Also, the antibacterial properties of the construct were evaluated by seeding the construct with antibacterial agents, such as silver nanoparticles, titanium dioxide and chlorhexidine diacetate.

In the third part, cell interactions with biomaterials were studied. We cultured embryonic rat skeletal muscle and motoneuron cells together on a patterned silicon based micro-cantilever device. The culture was then maintained in a defined medium and after 10-12 days in culture, the system was interrogated with an AFM detection system. The muscle contraction dynamics on application of defined external electrical field stimulation was recorded. We also attempted to show the existence of an *in-vitro* neuro-muscular junction with the help of the neurotransmitter glutamate.

In the future, work involves using more sensitive detection methods for quantifying protein adsorption and also using our cantilever based system as a high-throughput drug-screening platform.